Available online at www.jourcc.com

Journal homepage: www.JOURCC.com

Journal of Composites and Compounds

# Effect of $MgF_2$ addition on the mechanical properties of hydroxyapatite synthesized via powder metallurgy

*Amirhossein Shahbaz [a]*, Mohammad Esmaeilian [b], Reyhaneh Nasr Azadani [c], Kiana Gavanji [d]*

[a] *Materials Engineering, Saveh Islamic Azad University, Saveh, Iran*

[b] *Research Institute for Advanced Materials and New Energy, Iran Scientific and Industrial Research Organization, Tehran, Iran*

[c] *Department of Biomaterials Nanotechnology and Tissue engineering, Isfahan University of Medical Sciences, Isfahan, Iran*

[d] *Department of Medical Nanotechnology, School of Advanced Technologies in Medicine, Tehran University of Medical Sciences (TUMS), Tehran, Iran*

A B S T R A C T

Hydroxyapatite, a type of bioceramics, is mainly used as an implant for hard tissues due to its similarity to the structure of hard tissues. The aim of this study is to improve the mechanical properties of hydroxyapatite for biological uses. For this purpose the effect of magnesium fluoride ($MgF_2$) addition with different weight percentages (0, 5, 7.5 and 10 wt. %) on the mechanical properties of pure hydroxyapatite sintered at various temperatures (900, 1000 and 1100 °C) was investigated. XRD analysis was performed to study the decomposition of hydroxyapatite and the transformed phases. The density, Vickers microhardness and fracture toughness of the specimens were measured. The SEM analysis was performed to investigate the microstructure of samples. The results showed that the decomposition of hydroxyapatite to tri-calcium phosphate (TCP) decreased with increasing $MgF_2$. Also, an increment in density and mechanical properties of the specimens were observed with increasing the amount of hydroxyapatite. The fracture toughness of sintered pure hydroxyapatite increased from 2.3 to 1.3 MPa.$m^{1/2}$. The specimen containing 10 wt. % $MgF_2$ sintered at 1100 °C showed the best mechanical properties.



Peer review under responsibility of JCC Research Group.

A R T I C L E I N F O R M A T I O N

*Article history:*
Received 16 August 2019
Received in revised form 27 September 2019
Accepted 2 December 2019

*Keywords:*
Hydroxyapatite
Magnesium Fluoride ($MgF_2$)
Tri-Calcium Phosphate (TCP)
Sinter

## 1. Introduction

Hydroxyapatite (HA), with the chemical composition of $Ca_{10}(PO_4)_6(OH)_2$ [1, 2], due to its similarity to inorganic sections of bone and biocompatibility, is an important material in bone replacement as well as implants for hard tissues. HA is used in various fields such as biomedical applications [3-8]. Due to poor mechanical properties of HA, especially low flexural strength and fracture toughness, its uses are limited to applications with no mechanical stress or low stress [9-14]. Therefore, efforts have been made to improve the mechanical properties of HA-based implants [15-24].

During the sintering process of HA, it decomposes to TCP or tetra-calcium phosphate phases (reactions (1) and (2)) [10, 25].

$$Ca_{10}(PO_4)_6(OH)_2 \rightarrow 2Ca_3(PO_4)_2 + Ca_4P_2O_9 + H_2O \quad (1)$$

$$Ca_{10}(PO_4)_6(OH)_2 \rightarrow 3Ca_3(PO_4)_2 + CaO + H_2O \quad (2)$$

These decomposition reactions may negatively affect the density and consequently the mechanical properties of HA, which is due to the formation of secondary phases and production of $H_2O$. Also, the formed secondary phases increase the tendency for crack growth and biodegradation of HA ceramics. Meanwhile, TCP formation due to its high solubility, reduces the properties of HA composites [26].

Moreover, the addition of additives during the sintering process leads to the prevention of the HA to TCP degradation, as well as improvement in its mechanical properties. Several researches have been performed to investigate the effect of various additives such as $MgF_2$ [9, 10, 13], $AlF_3$ [27], $NH_4F$ [28], MgO [29], $AgNO_3$ [30], $LiNO_3$ [26], $CaF_2$ [31] and etc. [32-36]. On the other hand, recently, attentions have been paid to the effect of different parameters e.g. temperature on HA properties [3, 37, 38]. In this regard, fluoride ion is known to be an important additive for HA. This is due to the substitution (or doping) of the $F^-$ with $OH^-$ presented in HA, which prevents the degradation of the HA or reduces the level of the decomposition to TCP. This results in the improvement of the mechanical properites. On the other hand, with entrance of $F^-$ into the HA network, fluorapatite is formed which has higher thermal and chemical stability than that of HA that also prevents tooth and bone decay [9, 10, 13, 25, 39].

Mechanical alloying is known to have various advantages such as low time consumption [40-45], facility of process, and effective prop-

* *Corresponding author: Amirhossein Shahbaz; E-mail: amirhosein.shahbaz@gmail.com*

*DOR: 20.1001.1.26765837.2019.1.1.3.2*
*https://doi.org/10.29252/jcc.1.1.3*

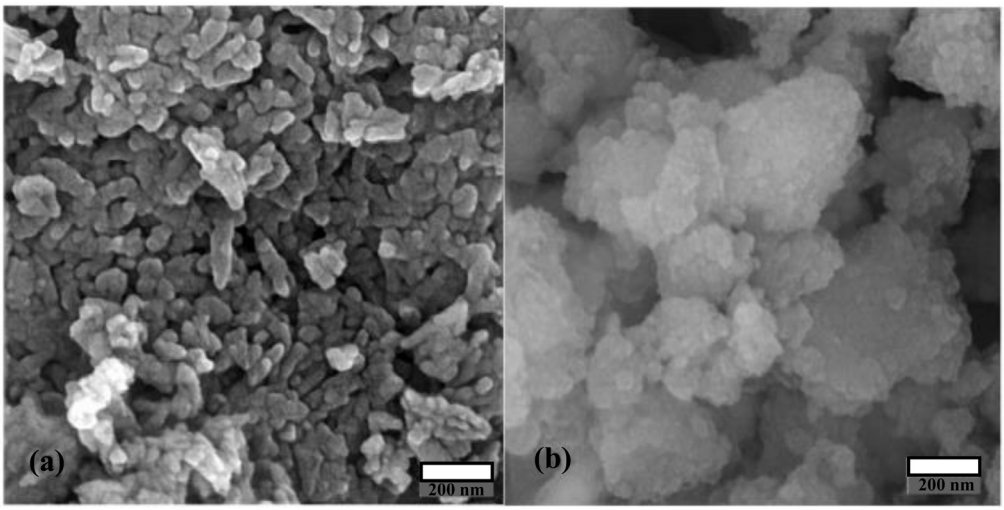


**Fig. 1.** SEM image of (a) HA powder and (b) primary $MgF_2$ powder.

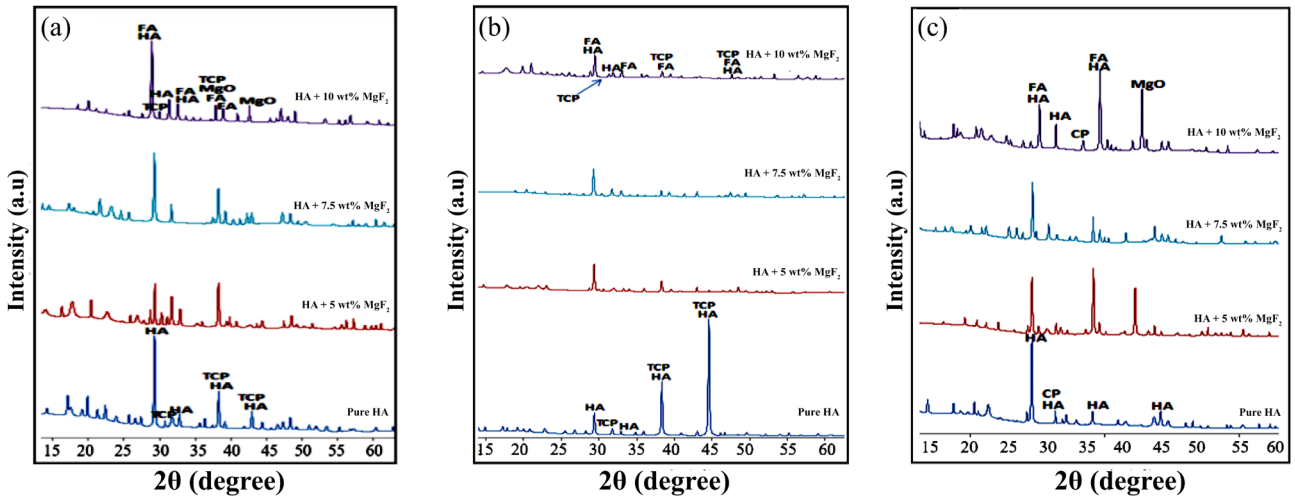


**Fig. 2.** X-ray diffraction spectra for specimens containing different percentages of $MgF_2$ sintered for 1 hour at (a) 900 °C, (b) 1000 °C, and (c) 1100 °C.

erties [46] that can be a good candidate to produce HA [47]. Although several research has been conducted to study the effect of adding $MgF_2$ to HA and its composites, further studies are required to investigate the effect $MgF_2$ addition to HA. Therefore, the aim of this study is to elucidate the effect of adding different amounts of the $MgF_2$ at different sintering temperatures on the mechanical properties and stability of HA as well as determining the optimum percentage of $MgF_2$ for preparing a biomaterial with desirable properties. For this purpose, $MgF_2$ with weight percentages of 5, 7.5 and 10 were added to HA and sintered at 900 to 1100 °C. Finally, the density, microstructure, hardness and fracture toughness of the specimens were evaluated.

## 2. Materials and methods

High purity HA powder (99.99%), the product of Aldrich Company, and $MgF_2$ powder of 97% purity from Analytical Fluka Company were provided. Fig. 1 shows the image of the purchased primary powders. Different weight percentages (5, 7.5 and 10 wt. %) of $MgF_2$ were added to HA. The mixtures containing HA and various amounts of $MgF_2$ were milled for 24 hours using alumina pellets. After the milling process, the mixtures were subjected to the cold isostatic press at 130 MPa. Then, they were sintered at temperatures of 900 to 1100 °C under airflow for 1 h without pressure.

The density of specimens was measured by the Archimedes method. The formed phases were evaluated after the sintering process using XRD analysis (INEL Equinox 3000). The test was performed by a diffractometry method using Cu-$K_\alpha$ irradiation (λ=1.54056 Å) under a voltage of 40 kV and a current of 30 mA. The specimens were evaluated at angles between 2θ of 15 and 65 degrees. In order to investigate the microstructure, the sections of the specimens were polished using diamond paste and etched. Finally, the microstructure of the specimens was examined by scanning electron microscopy (SEM, AIS 2300-seron Tech) with an accelerating voltage of 20 kV. The hardness of the specimens was measured by Vickers microhardness test method (MHV1000Z), which was performed under 200 g load on the polished surfaces of the specimens for 10 sec. The values of fracture toughness ($K_{IC}$) were calculated using the results obtained from the microhardness test based on Eq. (3) [48].

$$K_{IC} = 0.016 \left(\frac{E}{H_V}\right)^{0.5} \left(\frac{P}{C^{1.5}}\right) \quad (3)$$

Here, HV is Vickers hardness (GPa), P is the applied force (N), E is the modulus of elasticity (GPa) and C is the crack length (m). The crack length was measured immediately by a calibrated optical microscope.

## 3. Results and Discussion

### *3.1. Phase Analysis*

XRD analysis was used to evaluate the degradation of HA as well as determining the formed phases. Fig. 2 shows the X-ray diffraction for different percentages of $MgF_2$ at different sintering times.

Fig. 2 shows that HA and TCP are the main phases in the structure,

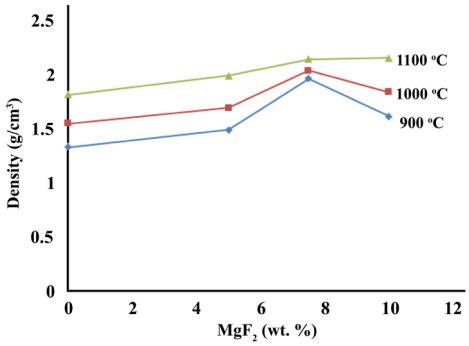


**Fig. 3.** Density variations of the specimens as percentage of $MgF_2$ at different temperatures of sintering.

while $MgF_2$ does not exist in the structure after the sintering process. This indicates that the decomposition of HA to TCP occurs due to sintering process.

The XRD spectra depicts that by the addition of $MgF_2$ to HA, the fluorapatite phase is also formed in the structure and after the sintering process, the phases of HA, TCP, fluorapatite and MgO are presented in the structure. The formation of the fluorapatite phase is because of $F^-$ substitution instead of $OH^-$ ions in the HA structure according to reaction (4).

$$Ca_{10}(PO_4)_6(OH)_2 + MgF_2 \rightarrow Ca_{10}(PO_4)_6F_2 + MgO + H_2O \quad (4)$$

Also, in order to evaluate the degradation rate of HA, it is necessary to check the intensity of HA and TCP peaks. To determine the HA decomposition into TCP, the relative values of the phases can be determined from the most extreme HA and TCP peaks. In fact, it is assumed that the concentrations of the HA and TCP phases are proportional to the height of their peaks in the mixture [10]. The rate of TCP formation in structures containing HA and TCP can be calculated using Eq. (5) [32].

$$\text{the fraction of decomposed } HA = I_{TCP}/(I_{TCP}+I_{HA}) \quad (5)$$

where $I_{TCP}$ is the peak intensity of the plane (0210) of the TCP phase and $I_{HA}$ is the peak intensity of the plane (211) of HA. Using this equation, the percentage of HA decomposed into calcium phosphate can be determined. Clearly, the greater the value obtained from this relationship, the greater the decomposition. These values were calculated for different specimens and listed in Table 1.

According to calculations based on Eq. 5, the most appropriate sintering temperature for 5 and 7.5 wt. % $MgF_2$ was 900 °C, while for the specimen with 10 wt.% $MgF_2$, sintering temperature of 1100 °C was suitable, in which, the lowest decomposition of 1.82 was observed. It should be noted that as the sintering temperature increased, the decomposition of pure HA significantly increased. The main reason for the decrease in the amount of degradation in the presence of fluorides is decomposition of $MgF_2$. As a result of this decomposition, $F^-$ is released and replaced in the HA structure by the $OH^-$ [9]. As a result of $MgF_2$ decomposition and reaction (4), a more stable phase of fluorapatite is formed and thus the decomposition of HA to TCP is reduced. Fluoride ions enhance the stability of the HA crystalline structure [13], and HA doped with F (fluorapatite) is more resistant to decomposition during sintering at high temperature than pure HA. According to Table 1, the higher the percentage of $MgF_2$ in the structure, the lower the degradation of HA to TCP and the more stable HA. As can be seen, the specimen containing 10 wt. % $MgF_2$ has only ~2 % of the decomposed-HA to TCP, and hence, HA stability is significantly increased. The main reason for this could be higher $F^-$ ions due to presence of higher $MgF_2$ content presented in the HA structure and consequently the reaction (4) occurs more, and higher fluorapatite is formed, thus the decomposition of HA to TCP is more prevented.

It should be noted that for samples from 7.5 to 10 wt. %, the degradation is increased. The reason for the negative effect of adding more than specific amount of $MgF_2$ on the stability of HA is that the excess $MgF_2$ does not participate in the formation of fluorapatite and is not visible in the X-ray diffraction (XRD) pattern because of its low content. This

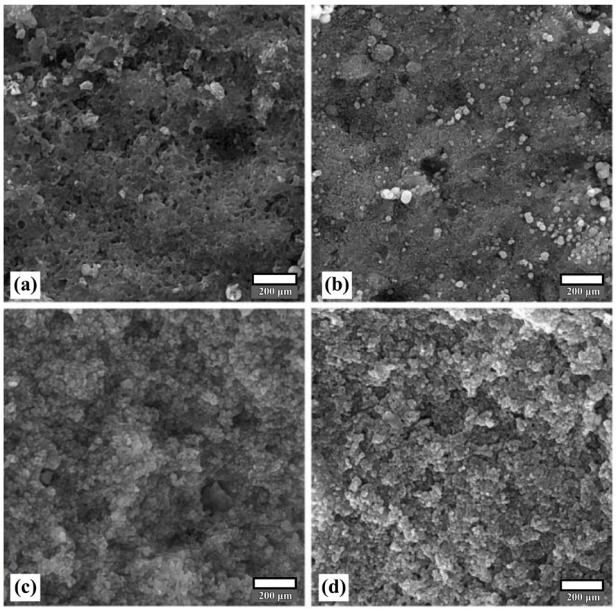


**Fig. 4.** SEM images of sintered specimens at 900 °C: (a) 0 wt. % $MgF_2$; b) 5 wt. % MgF2; c) 7.5 wt. % $MgF_2$; d) 10 wt. % $MgF_2$.

excess $MgF_2$ forms eutectic melt at the reaction temperatures with HA or TCP. In fact, the relative coarsening of the grains and porosities with the addition of higher amounts of $MgF_2$ indicates the possibility of eutectic melt formation. This has been observed in other works [13, 49].

### *3.2. Density*

The density values obtained for the specimens at different temperatures are presented in Fig. 3. Accordingly, the $MgF_2$-free specimen has the lowest density compared to other specimens. It can be noted that in the presence of $MgF_2$, the phase decomposition of HA into secondary phases i.e. TCP is reduced that leads to higher density. The reason for the higher density due to lower HA degradation is the production of $H_2O$ by decomposition of HA to TCP (reactions (1) and (2)). The produced $H_2O$ results in porosity. On the other hand, by decreasing the amount of HA decomposition in the presence of $MgF_2$, less $H_2O$ and porosity in the structure is produced and hence the density increases [9, 10]. It was also observed that by increasing the $MgF_2$ content, the density increases. According to Table 1, HA decomposition decreases with an increasing percentage of $MgF_2$. Additionally, the reduction of HA decomposition during sintering, reduces the amount of $H_2O$ formed by HA decomposition and thus reduces the porosity of the sintered specimens. As a result, when HA decomposition becomes lower, the removal of porosity in the final sintering stages becomes easier, which results in a highly dense structure [10].

The TCP phase resulted from the decomposition of HA has a lower density. As a result, specimens with higher TCP phase have lower density [13]. Also, substitution of $OH^-$ with $F^-$ (reaction (4)) results in $H_2O$ production. Replacement occurs below sintering temperature (below 1100 ° C). The $H_2O$ produced in this reaction vaporizes and discharges from the powder mixture and fluorapatite is formed ($Ca_{10}(PO_4)_6F_2$) [9].

**Table 1.**
Percentage of HA decomposed to TCP

| Percentage of decomposed HA (%) | $MgF_2$ (wt. %) |
|---|---|
| 86.31 | 0 |
| 58.97 | 5 |
| 33.24 | 7.5 |
| 1.82 | 10 |

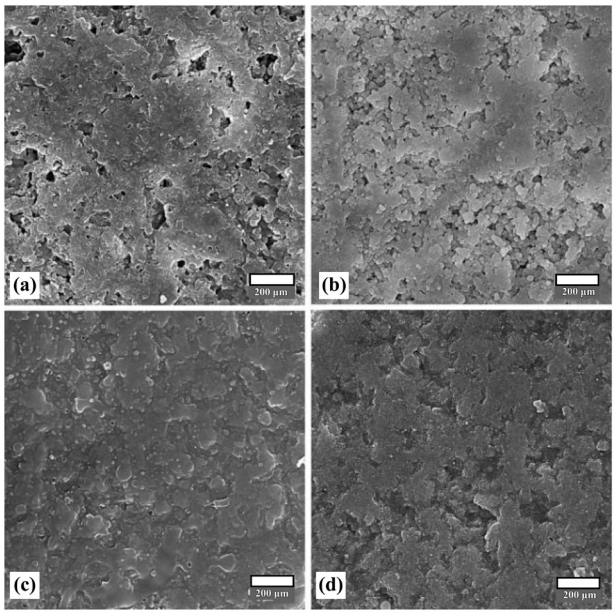


**Fig. 5.** SEM images of sintered specimens at 1000 °C: (a) 0 wt.% $MgF_2$; b) 5 wt.% $MgF_2$; c) 7.5 wt.% $MgF_2$; d) 10 wt.% $MgF_2$.

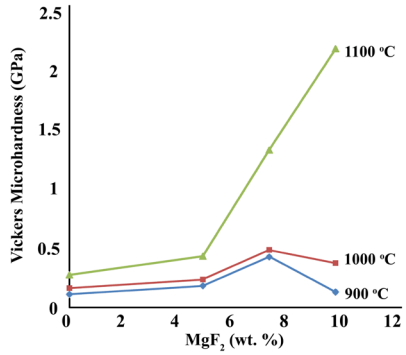


**Fig. 7.** Micro hardness values by weight percent of $MgF_2$ at different temperatures.

At two temperatures of 900 °C and 1000 °C, the density decreased with increasing $MgF_2$ from 7.5 to 10 wt% (Fig. 3). Given that the variations in density with $MgF_2$ percentage depend on the variations in the decomposition rate of HA, the cause of the decrease in the density of these specimens can be attributed to the increase in HA decomposition. However, $H_2O$ is also produced by the replacement of $F^-$ with $OH^-$ (reaction 3-4). But this replacement occurs at lower temperatures. Thus, the $H_2O$ produced in this reaction vaporizes and discharges from the powder mixture and leads to the fluorapatite ($Ca_{10}(PO_4)_6F_2$) formation [10].

By increasing the sintering temperature from 900 to 1100 °C, the density increases. The reason for this is that as the sintering temperature increases, the surface melting of the powder particles increases, which leads to higher density of the material [50]. It should be noted that although the increase in sintering temperature facilitates sintering due to improved surface melting and allowing more densification during sintering, this increase in temperature also facilitates phase decomposition of HA and leads to a higher rate of HA decomposition. According to abovementioned points, HA decomposition has a negative effect on the density and properties of HA-containing materials. Therefore, a temperature should be chosen for sintering at which the density is not reduced. It was observed that by increasing the temperature from 900 °C to 1100 °C, although the rate of HA decomposition increased (Fig. 3), the condensation is also increased. It can be implied that with increasing temperature, the improvement of sintering has been dominant over the increase in the decomposition rate and resulting in higher density. Increasing the density of HA specimens due to increment of sintering temperature has also been reported by Z. Evis et al. [10].

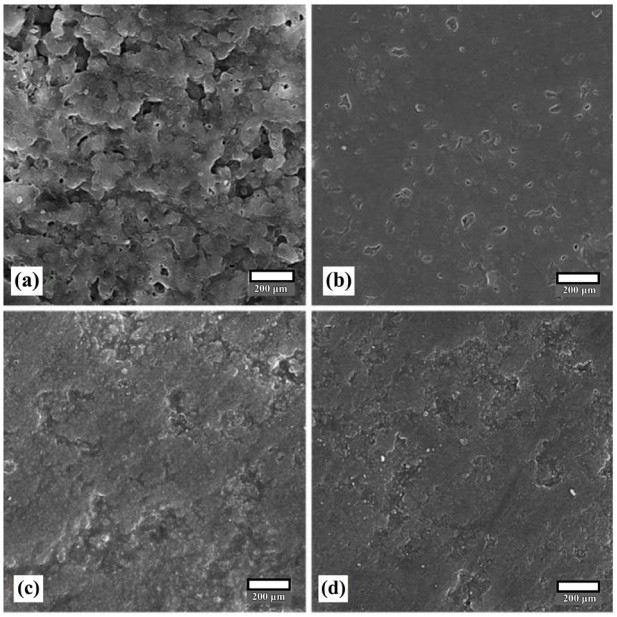


**Fig. 6.** SEM images of sintered specimens at 1100 °C: (a) 0 wt.% $MgF_2$; b) 5 wt.% $MgF_2$; c) 7.5 wt.% $MgF_2$; d) 10 wt.% $MgF_2$.

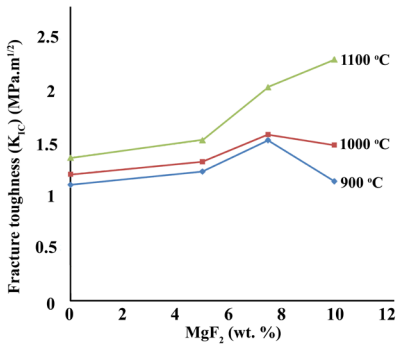


**Fig. 8.** Fracture toughness variations as a function of $MgF_2$ content at different temperatures.

*3.3. Microstructure*

SEM images of the specimens at different temperatures are presented in Figs. 4-6. Accordingly, the amount of porosity in the specimens decreased with increasing $MgF_2$ and the pores became smaller. As stated, the decomposition of HA to TCP decreases with increasing $MgF_2$ and thus the $H_2O$ produced by this phase decomposition also decreases. This reduces the porosity of the sintered specimens, that has been reported by other researchers [9, 10]. In fact, SEM images confirm the trend obtained for density variations.

According to Figs. 4-6, the increase in sintering temperature leads to a decrease in porosity in the structure. The reason is that sintering process improves with increasing temperature. Comparing the figures, it can be said that more surface melting at sintering temperatures of 1000 °C and 1100 °C is occurred compared to 900 °C. At temperatures of 1000 °C and 1100 °C, the particles and the grains are more difficult to separate and are more interconnected. However, it should be considered that in the specimens that have been sintered at higher temperatures (1000 °C and 1100 °C), porosities are relatively coarser. These are due to the higher phase decomposition of HA at these temperatures. As mentioned, increasing the temperature on one hand increases the phase decomposition and on the other hand, allows for higher densities to facilitate sintering. Although sintering improvement was dominant at this temperature range and resulted in a decrease in the overall porosity as well as increasing the density, due to more $H_2O$ production during the HA decomposition, the size of porosities in the $MgF_2$-free specimens was larger than that of 900 °C. However, as can be seen in Fig. 4 to 6, this did not occur at higher $MgF_2$ percentages. Generally, these results

confirm the trend for density variations in the specimens and other researches [51, 52].

*3.4. Hardness and Fracture Toughness*

As stated, the most important reason for the use of additives such as $MgF_2$ in HA materials is their effect on improving the mechanical properties of HA, which improves its usability in fields requiring mechanical load bearings. Both hardness and fracture toughness are two important mechanical properties that should be studied. The variation of microhardness as a function of $MgF_2$ percentage is shown in Fig. 7.

The fracture toughness of the specimens was calculated using Eq. 3 and its variation in terms of $MgF_2$ content is shown in Fig. 8. The obtained results of the hardness and fracture toughness show that by the addition of $MgF_2$ to HA, the hardness and fracture toughness increase. The fracture toughness of $MgF_2$-free HA sample is approximately 1.3 $MPa.m^{1/2}$, while by addition of $MgF_2$ it was increased to 2.3 $MPa.m^{1/2}$, which is significantly high.

The higher the amount of $MgF_2$, the greater the hardness and fracture toughness, especially at 7.5% and 10 wt. %. The reason for this increase can be attributed to the improvement in the density of the specimen by increasing the amount of $MgF_2$. The higher density or the lower porosity leads to the higher structural connection and the greater resistance to mechanical loading. Fracture toughness indicates the material resistance to the formation and growth of cracks. When there is a greater potential for crack growth in the material, less fracture toughness or energy absorption is obtained in the sample before fracture. Therefore, the presence of porosity in the material results in reduced fracture toughness.

Generally, the hardness and fracture toughness of HA specimens are depended on the density and porosity. Higher density due to lower phase decomposition of HA or improving the sintering by optimizing the effective parameters such as temperature is achieved. The dependence of hardness and fracture toughness on porosity has also been reported by other researchers [9, 10, 13].

## 4. Conclusions

In the present study, $MgF_2$ with values of 5, 7.5 and 10 wt % was added to HA. The powders were milled and sintered at various temperatures for one hour after cold pressing. The most important results of this study are as follows:

1. The addition of $MgF_2$, due to the substitution of $F^-$ with $OH^-$ in the structure of HA, resulted in the formation of a more stable fluorapatite phase, thus reducing the phase decomposition of HA to TCP.
2. Increasing the amount of $MgF_2$ led to lower phase decomposition resulted in an increase in density, and consequently an increase in hardness and fracture toughness.
3. Increasing the sintering temperature resulted in an increase in the amount of HA phase decomposition, while the structure became denser i.e. better mechanical properties.
4. The best amount of $MgF_2$ to reduce the phase decomposition and achieve the desired density and properties, depends on the sintering temperature. The optimum amount of $MgF_2$ is 10 wt% for the temperature of 1100˚C and 7.5 wt% for the temperatures of 900 ˚C and 1000 ˚C.
5. Fracture toughness values increased from 1.3 $MPa.m^{1/2}$ for pure sintered HA to 2.3 $MPa.m^{1/2}$, respectively.
6. Maximum density, hardness and fracture toughness were obtained for sintering temperature of 1100 °C at 10 wt.% $MgF_2$.

## Acknowledgments

The authors thank the University of Saveh Islamic Azad University, Saveh, Iran, for its financial and other support.

## Conflict of Interest

All authors declare no conflicts of interest in this paper.

REFERENCES

[1] A. Esmaeilkhanian, F. Sharifianjazi, A. Abouchenari, A. Rouhani, N. Parvin, M. Irani, Synthesis and Characterization of Natural Nano-hydroxyapatite Derived from Turkey Femur-Bone Waste, Applied Biochemistry and Biotechnology 189(3) (2019) 919-932.

[2] N.A.S. Mohd Pu'ad, P. Koshy, H.Z. Abdullah, M.I. Idris, T.C. Lee, Syntheses of hydroxyapatite from natural sources, Heliyon 5(5) (2019) e01588.

[3] S.K. Hubadillah, M.H.D. Othman, Z.S. Tai, M.R. Jamalludin, N.K. Yusuf, A. Ahmad, M.A. Rahman, J. Jaafar, S.H.S.A. Kadir, Z. Harun, Novel hydroxyapa-tite-based bio-ceramic hollow fiber membrane derived from waste cow bone for textile wastewater treatment, Chemical Engineering Journal 379 (2020) 122396.

[4] F. Sharifianjazi, N. Parvin, M. Tahriri, Formation of apatite nano-needles on novel gel derived $SiO_2$-$P_2O_5$-CaO-SrO-$Ag_2O$ bioactive glasses, Ceramics Interna-tional 43(17) (2017) 15214-15220.

[5] E. Sharifi Sedeh, S. Mirdamadi, F. Sharifianjazi, M. Tahriri, Synthesis and evaluation of mechanical and biological properties of scaffold prepared from Ti and Mg with different volume percent, Synthesis and Reactivity in Inorganic, Met-al-Organic, and Nano-Metal Chemistry 45(7) (2015) 1087-1091.

[6] A. Moghanian, A. Ghorbanoghli, M. Kazem-Rostami, A. Pazhouheshgar, E. Salari, M. Saghafi Yazdi, T. Alimardani, H. Jahani, F. Sharifian Jazi, M. Tahriri, Novel antibacterial Cu/Mg-substituted 58S-bioglass: Synthesis, characterization and investigation of in vitro bioactivity, International Journal of Applied Glass Science 11(4) (2020) 685-698.

[7] B.Y.S. Kumar, A.M. Isloor, G.C.M. Kumar, Inamuddin, A.M. Asiri, Nano-hy-droxyapatite Reinforced Chitosan Composite Hydrogel with Tunable Mechanical and Biological Properties for Cartilage Regeneration, Scientific Reports 9(1) (2019) 15957.

[8] C.C. Coelho, L. Grenho, P.S. Gomes, P.A. Quadros, M.H. Fernandes, Nano-hydroxyapatite in oral care cosmetics: characterization and cytotoxicity assessment, Scientific Reports 9(1) (2019) 11050.

[9] Z. Evis, R.H. Doremus, Effect of $AlF_3$, $CaF_2$ and $MgF_2$ on hot-pressed hydroxy-apatite–nanophase alpha-alumina composites, Materials Research Bulletin 43(10) (2008) 2643-2651.

[10] Z. Evis, M. Usta, I. Kutbay, Hydroxyapatite and zirconia composites: Effect of MgO and $MgF_2$ on the stability of phases and sinterability, Materials Chemistry and Physics 110(1) (2008) 68-75.

[11] M. Fanovich, M. Castro, J.P. Lopez, Improvement of the microstructure and microhardness of hydroxyapatite ceramics by addition of lithium, Materials Letters 33(5-6) (1998) 269-272.

[12] D.S. Gomes, A.M.C. Santos, G.A. Neves, R.R. Menezes, A brief review on hydroxyapatite production and use in biomedicine, Cerâmica 65 (2019) 282-302.

[13] S.-J. Kim, H.-G. Bang, J.-H. Song, S.-Y. Park, Effect of fluoride additive on the mechanical properties of hydroxyapatite/alumina composites, Ceramics International 35(4) (2009) 1647-1650.

[14] Y. Shinno, T. Ishimoto, M. Saito, R. Uemura, M. Arino, K. Marumo, T. Nakano, M. Hayashi, Comprehensive analyses of how tubule occlusion and advanced glycation end-products diminish strength of aged dentin, Scientific Reports 6(1) (2016) 19849.

[15] P. Abasian, M. Radmansouri, M. Habibi Jouybari, M.V. Ghasemi, A. Moham-madi, M. Irani, F.S. Jazi, Incorporation of magnetic NaX zeolite/DOX into the PLA/chitosan nanofibers for sustained release of doxorubicin against carcinoma cells death in vitro, International Journal of Biological Macromolecules 121 (2019) 398-406.

[16] M.M. Aliasghar Abuchenari, The Effect of Cu-Substitution on the Microstruc-ture and Magnetic Properties of Fe-15%Ni alloy Prepared by Mechanical Alloying composites and compounds 1(1) (2019) 13-19.

[17] M. Ekrami, J. Shahbazi Karami, A. Araee, F. Sharifianjazi, E. Sadeghi, A. Moghanian, Fabrication of copper/stainless steel bimetallic couple, by diffusion bonding using silver and nickel foils as interlayers, Inorganic and Nano-Metal Chemistry 49(5) (2019) 152-162.

[18] Z. Goudarzi, N. Parvin, F. Sharifianjazi, Formation of hydroxyapatite on surface of $SiO_2$– $P_2O_5$–CaO–SrO–ZnO bioactive glass synthesized through sol-gel

route, Ceramics International 45(15) (2019) 19323-19330.
[19] M.S. Leila Bazli, Arman Shiravi, A Review of Carbon Nanotube/$TiO_2$ Composite Prepared via Sol-Gel Method compsites and compounds 1(1) (2019) 1-12.
[20] A. Moghanian, F. Sharifianjazi, P. Abachi, E. Sadeghi, H. Jafarikhorami, A. Sedghi, Production and properties of Cu/$TiO_2$ nano-composites, Journal of Alloys and Compounds 698 (2017) 518-524.
[21] M. Radmansouri, E. Bahmani, E. Sarikhani, K. Rahmani, F. Sharifianjazi, M. Irani, Doxorubicin hydrochloride - Loaded electrospun chitosan/cobalt ferrite/tita-nium oxide nanofibers for hyperthermic tumor cell treatment and controlled drug release, International Journal of Biological Macromolecules 116 (2018) 378-384.
[22] V. Salimian Rizi, F. Sharifianjazi, H. Jafarikhorami, N. Parvin, L. Saei Fard, M. Irani, A. Esmaeilkhanian, Sol–gel derived $SnO_2$/$Ag_2O$ ceramic nanocomposite for $H_2$ gas sensing applications, Materials Research Express 6(11) (2019) 1150g2.
[23] M.S.N. Shahrbabak, F. Sharifianjazi, D. Rahban, A. Salimi, A Comparative Investigation on Bioactivity and Antibacterial Properties of Sol-Gel Derived 58S Bioactive Glass Substituted by Ag and Zn, Silicon 11(6) (2019) 2741-2751.
[24] F. Sharifianjazi, N. Parvin, M. Tahriri, Synthesis and characteristics of sol-gel bioactive $SiO_2$-$P_2O_5$-CaO-$Ag_2O$ glasses, Journal of Non-Crystalline Solids 476 (2017) 108-113.
[25] Z. Evis, M. Usta, I. Kutbay, Improvement in sinterability and phase stability of hydroxyapatite and partially stabilized zirconia composites, Journal of the Eu-ropean Ceramic Society 29(4) (2009) 621-628.
[26] Y. Luo, D. Li, J. Zhao, Z. Yang, P. Kang, In vivo evaluation of porous lithium-doped hydroxyapatite scaffolds for the treatment of bone defect, Bio-medical materials and engineering (Preprint) (2018) 1-23.
[27] K. Hua, X. Xi, L. Xu, K. Zhao, J. Wu, A. Shui, Effects of $AlF_3$ and $MoO_3$ on properties of Mullite whisker reinforced porous ceramics fabricated from construc-tion waste, Ceramics International 42(15) (2016) 17179-17184.
[28] S.S. Rahavi, O. Ghaderi, A. Monshi, M.H. Fathi, A comparative study on physicochemical properties of hydroxyapatite powders derived from natural and synthetic sources, Russian Journal of Non-Ferrous Metals 58(3) (2017) 276-286.
[29] K. Kowalski, M.U. Jurczyk, P.K. Wirstlein, J. Jakubowicz, M. Jurczyk, Prop-erties of ultrafine-grained Mg-based composites modified by addition of silver and hydroxyapatite, Materials Science and Technology 34(9) (2018) 1096-1103.
[30] H.X. Chen, F. Xue, D. Yang, Y.Z. Qiufen, Hydrothermal synthesis and char-acterization of Ag-doped hydroxyapatite antibacterial agent, Acta Chimica Sinica 70(12) (2012) 1362-1366.
[31] H.-W. Kim, Y.-H. Koh, S.-B. Seo, H.-E. Kim, Properties of fluoridated hy-droxyapatite–alumina biological composites densified with addition of $CaF_2$, Ma-terials Science and Engineering: C 23(4) (2003) 515-521.
[32] I. Manjubala, T. Sampath Kumar, Preparation of biphasic calcium phosphate doped with magnesium fluoride for osteoporotic applications, Journal of materials science letters 20(13) (2001) 1225-1227.
[33] M. Turkoz, A.O. Atilla, Z. Evis, Silver and fluoride doped hydroxyapatites: investigation by microstructure, mechanical and antibacterial properties, Ceramics International 39(8) (2013) 8925-8931.
[34] C.-C. Wu, S.-T. Huang, T.-W. Tseng, Q.-L. Rao, H.-C. Lin, FT-IR and XRD investigations on sintered fluoridated hydroxyapatite composites, Journal of Mo-lecular Structure 979(1-3) (2010) 72-76.
[35] B. Bakhshandeh, M. Soleimani, N. Ghaemi, I. Shabani, Effective combination of aligned nanocomposite nanofibers and human unrestricted somatic stem cells for bone tissue engineering, Acta Pharmacologica Sinica 32(5) (2011) 626-636.
[36] E. Nogami, I. Watanabe, H. Hoshi, M. Kasahara, N. Honda, M. Sato, K. Suzu-ki, D-sorbitol can keep the viscosity of dispersive ophthalmic viscosurgical device at room temperature for long term, Scientific Reports 9(1) (2019) 16815.
[37] M. Ibrahim, M. Labaki, J.-M. Giraudon, J.-F. Lamonier, Hydroxyapatite, a multifunctional material for air, water and soil pollution control: A review, Journal of Hazardous Materials 383 (2020) 121139.
[38] D.O. Obada, E.T. Dauda, J.K. Abifarin, D. Dodoo-Arhin, N.D. Bansod, Me-chanical properties of natural hydroxyapatite using low cold compaction pressure: Effect of sintering temperature, Materials Chemistry and Physics 239 (2020) 122099.
[39] X. Li, J. Zhu, Z. Man, Y. Ao, H. Chen, Investigation on the structure and upconversion fluorescence of $Yb^{3+}$/$Ho^{3+}$ co-doped fluorapatite crystals for potential biomedical applications, Scientific Reports 4(1) (2014) 4446.
[40] E.H. Jazi, R. Esalmi-Farsani, G. Borhani, F.S. Jazi, Synthesis and Character-ization of In Situ Al-$Al_{13}Fe_4$-$Al_2O_3$-$TiB_2$ Nanocomposite Powder by Mechanical Alloying and Subsequent Heat Treatment, Synthesis and Reactivity in Inorganic, Metal-Organic, and Nano-Metal Chemistry 44(2) (2014) 177-184.
[41] A. Masoudian, M. Karbasi, F. SharifianJazi, A. Saidi, Developing $Al_2O_3$-TiC in-situ nanocomposite by SHS and analyzingtheeffects of Al content and mechanical activation on microstructure, Journal of Ceramic Processing Research 14(4) (2013) 486-491.
[42] C. Kursun, M. Gogebakan, E. Uludag, M.S. Bozgeyik, F.S. Uludag, Structural, electrical and magnetic properties of Nd – A – $CoO_3$ (A = Sr, Ca) Perovskite Powders by Mechanical Alloying, Scientific Reports 8(1) (2018) 13083.
[43] M.S. Mustaffa, R.a.S. Azis, N.H. Abdullah, I. Ismail, I.R. Ibrahim, An investi-gation of microstructural, magnetic and microwave absorption properties of multi-walled carbon nanotubes/$Ni_{0.5}Zn_{0.5}Fe_2O_4$, Scientific Reports 9(1) (2019) 15523.
[44] Y.-J. Hu, J. Li, K.A. Darling, W.Y. Wang, B.K. VanLeeuwen, X.L. Liu, L.J. Kecskes, E.C. Dickey, Z.-K. Liu, Nano-sized Superlattice Clusters Created by Oxygen Ordering in Mechanically Alloyed Fe Alloys, Scientific Reports 5(1) (2015) 11772.
[45] Asfandiyar, T.-R. Wei, Z. Li, F.-H. Sun, Y. Pan, C.-F. Wu, M.U. Farooq, H. Tang, F. Li, B. Li, J.-F. Li, Thermoelectric SnS and SnS-SnSe solid solutions prepared by mechanical alloying and spark plasma sintering: Anisotropic thermoelec-tric properties, Scientific Reports 7(1) (2017) 43262.
[46] V. Balouchi, F.S. Jazi, A. Saidi, Developing (W, Ti) C-(Ni, Co) nanocomposite by SHS method, Journal of Ceramic Processing Research 16(5) (2015) 605-608.
[47] M. Alizadeh, F. Sharifianjazi, E. Haghshenasjazi, M. Aghakhani, L. Rajabi, Production of nanosized boron oxide powder by high-energy ball milling, Synthe-sis and Reactivity in Inorganic, Metal-Organic, and Nano-Metal Chemistry 45(1) (2015) 11-14.
[48] J.J. Kruzic, D.K. Kim, K.J. Koester, R.O. Ritchie, Indentation techniques for evaluating the fracture toughness of biomaterials and hard tissues, Journal of the Mechanical Behavior of Biomedical Materials 2(4) (2009) 384-395.
[49] H.-W. Kim, Y.-J. Noh, Y.-H. Koh, H.-E. Kim, H.-M. Kim, Effect of $CaF_2$ on densification and properties of hydroxyapatite–zirconia composites for biomedical applications, Biomaterials 23(20) (2002) 4113-4121.
[50] A.R. Rouhani, A.H. Esmaeil-Khanian, F. Davar, S. Hasani, The effect of agarose content on the morphology, phase evolution, and magnetic properties of $CoFe_2O_4$ nanoparticles prepared by sol-gel autocombustion method, International Journal of Applied Ceramic Technology 15(3) (2018) 758-765.
[51] H. Ibrahim, S.N. Esfahani, B. Poorganji, D. Dean, M. Elahinia, Resorbable bone fixation alloys, forming, and post-fabrication treatments, Materials Science and Engineering: C 70 (2017) 870-888.
[52] I. Mutlu, Production and fluoride treatment of Mg-Ca-Zn-Co alloy foam for tissue engineering applications, Transactions of Nonferrous Metals Society of China 28(1) (2018) 114-124.